New Journal of Physics
The open access journal for physics

Dirac-cone-like surface state in W(110): dispersion, spin texture and photoemission from first principles

H Mirhosseini[1,3], M Flieger[2] and J Henk[2,3]

[1] Max Planck Institute of Microstructure Physics, Weinberg 2, D-06120 Halle, Saale, Germany

[2] Institute of Physics-Theoretical Physics, Martin Luther University Halle-Wittenberg, D-06099 Halle, Saale, Germany

E-mail: hossein@mpi-halle.mpg.de and juergen.henk@physik.uni-halle.de

New Journal of Physics **15** (2013) 033019 (16pp)
Received 19 October 2012
Published 15 March 2013
Online at http://www.njp.org/
doi:10.1088/1367-2630/15/3/033019

Abstract. We report on a theoretical study of a d_{z^2} surface state at the tungsten (110) surface, addressing in detail the spin-resolved electronic structure as well as photoemission spectroscopy. In agreement with recent experiments, this surface state shows a strongly anisotropic dispersion: in the $\overline{\mathrm{H}}$–$\overline{\Gamma}$–$\overline{\mathrm{H}}$ direction of the surface Brillouin zone, it disperses linearly but becomes flattened along the $\overline{\mathrm{N}}$–$\overline{\Gamma}$–$\overline{\mathrm{N}}$ direction. The *ab initio* calculated spin texture agrees with the one derived from a model Hamiltonian; due to twofold surface symmetry and time-reversal symmetry, the out-of-plane spin polarization vanishes. The photoemission intensities depend sensitively on the polarization of the incident light, because of the orbital composition of the surface state. The photoelectrons become spin-polarized out-of-plane, which is attributed to breaking the time-reversal symmetry by the excitation process.

[3] Authors to whom any correspondence should be addressed.

TH-2013-04

Contents

1. Introduction

Topological insulators are a class of materials whose properties are important for both fundamental physics and device applications (e.g. [1]). While insulating in the bulk, these solids show surface states with unique features: they bridge the fundamental band gap and show linear dispersion, similar to relativistic massless particles. The two branches of such a surface state that are related by time-reversal symmetry cross at a time-reversal invariant momentum [2]; this crossing point in energy E and momentum $\hbar\boldsymbol{k}$ is called a Dirac point. The spin–orbit interaction prescribes a specific spin texture of the Dirac surface states [3].

Inspired by the ground-breaking early investigations, mainly on HgTe systems [4] and bichalkogenides (e.g. Bi_2Se_3) [5], there is now an ongoing search for new topological insulators [6]. Means of transforming conventional insulators into topological insulators are, for example, lattice distortions [7] or substitutional disorder [8]. This quest has led also to the re-inspection of the surface states of materials that were believed well investigated and understood but cannot be transformed into a topological insulator: transition metals such as W(110) [9].

Recently, a surface state has been found on W(110) whose dispersion shows striking similarity to that of a Dirac surface state [9]. This finding is particularly astonishing since W(110) misses almost all ingredients of a true topological insulator (e.g. of the bichalkogenide type). (i) It is a metal and, thus, shows no fundamental band gap. However, it displays gaps in parts of the Brillouin zone below the Fermi energy. (ii) A band inversion across a fundamental band gap is missing. (iii) It is not a compound, in contrast to the topological insulators of the HgTe and Bi_2Se_3 types. (iv) The energy range of the observed surface state is populated by d electrons, in contrast to p electrons at the fundamental band gap in topological insulators. However, topological insulators and tungsten have in common a strong spin–orbit coupling: $Z = 74$ for *tungsten* (Swedish for 'heavy stone').

The 'Dirac surface state'[4] on W(110) is energetically situated in a partial band gap that is due to spin–orbit coupling, similar to the spin–orbit-induced fundamental band gap in a

[4] Although W is not a topological insulator and, hence, its surface state cannot be topologically protected (that is a 'true Dirac state'), we shall call this surface state deliberately a 'Dirac state' in this paper.

topological insulator. It shows a band crossing with linear dispersion, that is a Dirac point. However, while true Dirac states form a—more or less—isotropic two-dimensional electron gas (for warping of Dirac states see [3, 10]), the Dirac state of W(110) is highly anisotropic: in one direction of the two-dimensional Brillouin zone, it disperses linearly and strongly but becomes 'flattened' along the orthogonal direction. This finding is explained by the twofold symmetry of the W(110) surface [11].

It turns out that, to our knowledge, this special surface state has so far been investigated experimentally by means of spin- and angle-resolved photoelectron spectroscopy (SARPES) and by a model calculation [9, 11]. However, a comprehensive theoretical study by means of first-principles electronic structure calculations is missing. In this paper we report on such a theoretical investigation.

We show that all features of the Dirac state can be explained by the Rashba spin–orbit coupling [12, 13]. Our first-principles calculations predict a second surface state with lower binding energy and opposite spin polarization with respect to the Dirac state. The hybridization of the Dirac state and the surface state results in a maximum in the dispersion of the Dirac state that, as a consequence, does not bridge the band gap. These observations are similar to those in the Rashba systems Bi/Ag(111) [14] and Bi/Cu(111) [15]. There, the sp_z surface state hybridizes with a $p_x p_y$ surface state at higher energy and also opposite spin polarization [16]. In Bi/Cu(111), this hybridization even results in a spin reversal [15]. The spin polarization is entirely in-plane, as is explained by symmetry considerations.

In photoemission experiments, Miyamoto *et al* [11] found a strong dependence of the photoemission intensities on the light polarization. This feature has been convincingly explained by the orbital composition of the Dirac state. Nevertheless, such a finding calls for support by first-principles photoemission calculations that provide a direct link between the electronic structure calculations for the ground state and the experiments. Hence, we performed such computations within the relativistic one-step model of photoemission and confirm the experimental findings. On top of this, we address the spin polarization of the photoelectron and compare it with that of the Dirac state, using the experimental setups. It turns out that the photoelectron's spin can be tilted out-of-plane, although the spin of the Dirac surface state is in-plane; this finding is attributed to time-reversal breaking by the photoemission process.

The paper is organized as follows. Theoretical aspects are addressed in section 2. The results-and-discussion (section 3) comprises the analysis of the dispersion (section 3.1), the spin texture (section 3.2), as well as the spin- and angle-resolved photoemission (SARPES, section 3.3). Concluding remarks are given in section 4.

2. Theoretical aspects

In this section, we address the model Hamiltonian that is used for analyzing the basic properties of the Dirac state (section 2.1). Further, we give details on the first-principles electronic structure (section 2.2) and photoemission calculations (section 2.3).

2.1. Model Hamiltonian

Rashba-split surface states are well described by model Hamiltonians (see [3, 17] for Au(111) and bichalkogenide topological insulators, respectively). For the W(110) surface, we derived an analogous Hamiltonian from $\boldsymbol{k} \cdot \boldsymbol{p}$ perturbation theory [18], taking into account the twofold

Table 1. Effect of symmetry operations of the point group $2mm$ and of time reversal on the wavevector $\boldsymbol{k} = (k_x, k_y)$, the spin vector $\boldsymbol{s} = (s_x, s_y, s_z)$ and the vector potential $\boldsymbol{A} = (A_x, A_y, A_z)$ of the incident light (in photoemission). See also figure 1.

1	k_x	k_y	s_x	s_y	s_z	A_x	A_y	A_z	Identity
m_{xz}	k_x	$-k_y$	$-s_x$	s_y	$-s_z$	A_x	$-A_y$	A_z	Reflection at xz plane
m_{yz}	$-k_x$	k_y	s_x	$-s_y$	$-s_z$	$-A_x$	A_y	A_z	Reflection at yz plane
C_{2z}	$-k_x$	$-k_y$	$-s_x$	$-s_y$	s_z	$-A_x$	$-A_y$	A_z	z-rotation about π
T	$-k_x$	$-k_y$	$-s_x$	$-s_y$	$-s_z$	A_x	A_y	A_z	Time reversal

symmetry of this surface (point group $2mm$ [19]). This Hamiltonian agrees with that derived by Miyamoto *et al* [11]. The model Hamiltonian

$$H = H_0(\boldsymbol{k}) + H_{\mathrm{soc}}^{(1)}(\boldsymbol{k}) + H_{\mathrm{soc}}^{(3)}(\boldsymbol{k}), \quad \boldsymbol{k} = (k_x, k_y) \tag{1}$$

comprises three terms. (i) $H_0(\boldsymbol{k})$ describes the basic dispersion of an anisotropic two-dimensional electron gas without spin–orbit coupling,

$$H_0(\boldsymbol{k}) = \frac{\hbar^2 k_x^2}{2m_x^\star} + \frac{\hbar^2 k_y^2}{2m_y^\star}. \tag{2}$$

The effective masses $m_y^\star$ and $m_x^\star$ are $-4.7m_\mathrm{e}$ and $3.3m_\mathrm{e}$, respectively (electron mass m_e; all parameters in this section have been taken from [11]). (ii) $H_{\mathrm{soc}}^{(1)}(\boldsymbol{k})$ is the Rashba-type spin–orbit Hamiltonian in first order in the wavenumbers k_x and k_y,

$$H_{\mathrm{soc}}^{(1)}(\boldsymbol{k}) = \alpha_x k_x \sigma_y + \alpha_y k_y \sigma_x \tag{3}$$

with Pauli matrices σ_x and σ_y ($\alpha_x = -0.08\,\mathrm{eV\,\AA}$ and $\alpha_y = 1.05\,\mathrm{eV\,\AA}$). (iii) The contribution of third order to the spin–orbit coupling is given by

$$H_{\mathrm{soc}}^{(3)}(\boldsymbol{k}) = \alpha_{x^3} k_x^3 \sigma_y + \alpha_{x^2y} k_x^2 k_y \sigma_x + \alpha_{xy^2} k_x k_y^2 \sigma_y + \alpha_{y^3} k_y^3 \sigma_x \tag{4}$$

($\alpha_{x^3} = 5.57\,\mathrm{eV\,\AA^3}$, $\alpha_{x^2y} = 12.3\,\mathrm{eV\,\AA^3}$, $\alpha_{xy^2} = -25\,\mathrm{eV\,\AA^3}$ and $\alpha_{y^3} = 1.13\,\mathrm{eV\,\AA^3}$).

The above Hamiltonian reveals considerable differences with respect to those for systems with (111) surfaces [20, 21]. The latter surfaces show threefold rotational symmetry; their point group $3m$ (cf Au(111), Bi/Ag(111) and $Bi_2Te_3(111)$) implies $\alpha_x = -\alpha_y = \alpha_\mathrm{R}$ (Rashba parameter). Also the warping introduced by the third-order terms depends only on a single parameter [3]. Further, it tilts the spin polarization of the surface states out of the surface plane, as is described by the Pauli matrix σ_z. For a system with point group $2mm$, the two mirror planes that are perpendicular to each other allow, in principle, for an out-of-plane tilt. However, time-reversal symmetry forbids this because $E(\boldsymbol{k}, \boldsymbol{s}) = E(-\boldsymbol{k}, -\boldsymbol{s})$; compare the actions of C_{2z} and T on the spin vector $\boldsymbol{s}$ in table 1 which dictates $s_z \equiv 0$. Hence, the spin polarization vector $\boldsymbol{s}$ has to be in-plane for all wavevectors and $H_{\mathrm{soc}}^{(3)}(\boldsymbol{k})$ comprises only terms with σ_x and σ_y. Furthermore, for a wavevector parallel to the k_x-axis, the table yields $s_x \equiv 0$; thus, on the $\overline{\mathrm{N}}$–$\overline{\Gamma}$–$\overline{\mathrm{N}}$ line of the two-dimensional Brillouin zone (figure 1), only s_y is nonzero. Analogously, for $\boldsymbol{k}$ along the k_y-axis, one obtains $s_y \equiv 0$, which implies a nonzero s_x along the $\overline{\mathrm{N}}$–$\overline{\mathrm{H}}$–$\overline{\Gamma}$–$\overline{\mathrm{H}}$–$\overline{\mathrm{N}}$. These impositions are fully supported by our first-principles calculations.

This single-band approach leads to agreement of model and experiment in the energy region close to the Dirac point (band crossing at $k_x = k_y = 0$, $\overline{\Gamma}$). However, it does not hold

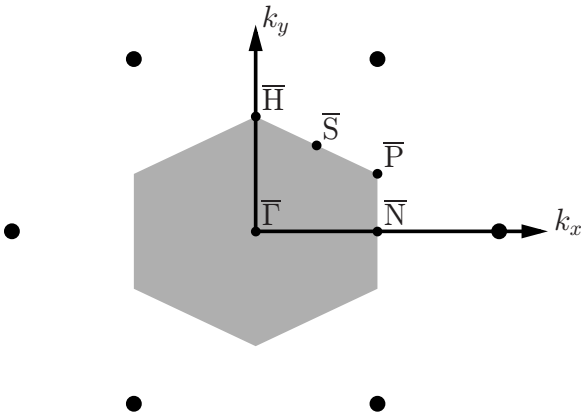

Figure 1. Reciprocal lattice of the W(110) surface. Lattice points are given by large filled circles. The first Brillouin zone is displayed in gray, with its high symmetry points marked by small filled circles. The k_x and the k_y axes are invariant under reflections m_{xz} and m_{yz}, respectively (see table 1).

at higher energies where—as we shall show below—the Dirac state hybridizes with another surface state (see also [15, 16]).

2.2. *First-principles electronic structure calculations*

We have performed *ab initio* calculations within the framework of the local density approximation to density functional theory. The electronic properties have been obtained by multiple-scattering computations with a relativistic layer Korringa–Kohn–Rostoker (KKR) code [22, 23]. Spin–orbit coupling is fully accounted for by solving the Dirac equation. The exchange-correlation functional is taken from [24].

The layer-resolved Green function $G_{ll}(E+\mathrm{i}\eta, \boldsymbol{k})$ provides detailed information on the electronic structure. l is the layer index, E the energy, η a small offset from the real energy axis and $\boldsymbol{k} = (k_x, k_y)$ is the in-plane wavevector. Both orbital composition and spin texture of the electronic states have been obtained from the spectral density [25]

$$N_l(E, \boldsymbol{k}) = -\frac{1}{\pi} \lim_{\eta \to 0^+} \mathrm{Tr}\, G_{ll}(E+\mathrm{i}\eta, \boldsymbol{k}) \tag{5}$$

by taking appropriate partial traces. A comparison of $N_l(E, \boldsymbol{k})$ for different layers l at fixed $(E, \boldsymbol{k})$ gives the localization of the surface states in the vacuum–surface region.

The spin textures of the electronic states are addressed by means of spin differences $s_\mu^\uparrow - s_\mu^\downarrow$ that are obtained from the spectral density in (5). The spin projections $\uparrow$ and $\downarrow$ are given with respect to the chosen spin quantization axis μ (e.g. $\mu = y$ for $\boldsymbol{k}$ on the k_x-axis).

The entire system comprises three regions: (i) semi-infinite bulk, (ii) the surface region that consists of six W layers and four layers of vacuum and (iii) semi-infinite vacuum. The image potential barrier is mimicked by the so-called empty muffin-tin spheres, rather than by a smooth interpolating function [26]. In a KKR calculation of the surface electronic structure of W(110) by Giebels *et al* [27], a smooth interpolating function is used as an image-potential barrier. We find no significant changes with respect to our calculation that uses empty muffin-tin spheres. The only exception is a slightly better binding energy of the

Dirac surface state in that calculation because of the adjustment of the barrier parameters. All other properties, in particular the spin polarization, agree very well. Bulk layers are denoted B, whereas surface layers are named S, S − 1, S − 2, etc, starting with the topmost surface layer S. Similarly, vacuum layers are Vac, Vac + 1, etc. The surface layer is relaxed toward the bulk by $\delta d_{12} = -2.75\%$ of the bulk interlayer distance, as has been obtained from the surface x-ray diffraction [28]. Low-energy electron diffraction (LEED) gives comparable contractions (e.g. -2.2% in [29]).

The layer KKR method relies on two representations for the electronic states: plane waves and spin-angular functions. The number of plane waves, used in the interlayer scattering, was at least 50. The maximum angular momentum, used in the single-site scattering and the intralayer scattering, was $l_{\max} = 3$. Both numbers guarantee converged results. The offset η from the real energy axis in (5) is 5 meV.

2.3. Photoemission calculations

We have also computed spin- and angle-resolved photoemission intensities within the relativistic one-step model of photoelectron spectroscopy [22, 30], using the potentials of the first-principles calculations as input. These theoretical spectra provide a direct link between the spectral density maps of the initial states (occupied states) and the measured intensity maps of the photoelectrons.

The spin-density matrix of the photoelectron is calculated from

$$\rho_{\sigma\sigma'}(E, \boldsymbol{k}) \propto \left\langle \Phi_\sigma(E, \boldsymbol{k}) | \Delta(\omega) G(E - \hbar\omega, \boldsymbol{k}) \Delta^\dagger(\omega) | \Phi_{\sigma'}(E, \boldsymbol{k}) \right\rangle, \quad \sigma, \sigma' = \uparrow, \downarrow, \tag{6}$$

which represents the triangular Feynman diagram of the one-step model of photoemission [31, 32]. The initial (occupied) electronic states are represented by the Green function $G(E - \hbar\omega, \boldsymbol{k})$. The dipole operator $\Delta(\omega) \propto \boldsymbol{\alpha} \cdot \boldsymbol{A}(\omega)$ mediates the transition from the initial state to the outgoing photoelectron state, that is the time-reversed LEED state $\Phi_\sigma(E, \boldsymbol{k})$ with spin projection σ. $\boldsymbol{\alpha}$ is a vector of Dirac matrices [33], while $\boldsymbol{A}(\omega)$ is the vector potential of the incident radiation with photon energy $\hbar\omega$.

The spin-averaged photocurrent is given by $I(E, \boldsymbol{k}) = \operatorname{tr} \rho(E, \boldsymbol{k})$, while the spin polarization of the photoelectrons reads

$$\boldsymbol{s}(E, \boldsymbol{k}) = \frac{\operatorname{tr}[\boldsymbol{\sigma}\, \rho(E, \boldsymbol{k})]}{I(E, \boldsymbol{k})} \tag{7}$$

($\boldsymbol{\sigma}$ is the vector of Pauli matrices). Due to spin–orbit coupling, the photocurrent is, in general, spin polarized even for nonmagnetic samples, depending on the specific setup (see [34] and references therein).

The above model takes into account the correct boundary conditions [35], the electronic structure above the vacuum level (via the time-reversed LEED state), dipole selection rules (via the dipole operators) and the electronic structure of the occupied states. The in-plane wavevector $\boldsymbol{k}$ is conserved due to translational invariance within the layers. Hence, it allows for *quantitative* comparison with experiments (see e.g. [17, 36]).

The photoemission calculations use the same setup as the electronic structure calculations. The Green function in (6) introduces a sum over all layers [37] which is approximated by a finite sum over the outermost layers. This is justified by the finite lifetime of the photoelectrons that introduces the surface sensitivity of photoelectron spectroscopy in the vacuum ultraviolet (VUV) range [38]. Here, the topmost 30 layers contribute to the photocurrent. The lifetime

broadening is mimicked by an imaginary part of the energy, taken as −0.025 eV for the occupied and −1.0 eV for the unoccupied states. These values are chosen to clearly show the spin texture of the Dirac-like surface states. However, for reproducing experimental spectra these values have to be optimized and have to be taken as energy dependent. The quality of our approach may be judged from the data shown in [36].

The setup is adopted from [9, 11] (see figure 1 in these publications). The optical plane is spanned by the surface normal, the direction of light incidence and the direction of photoelectron detection. The sample is rotated about the surface normal by an angle ϕ_e and the photoelectrons are detected at a polar angle θ_e. The polar angle θ_{ph} of light incidence is 50°. We use both completely s- and p-polarized light with a photon energy of 22.5 eV (as in the experiment).

3. Results and discussion

3.1. Dispersion

In the energy range that is relevant for the Dirac-like surface state, the W band structure shows a pocket-shaped partial band gap that is induced by spin–orbit coupling (top row in figure 2). This band gap is occupied by a strongly dispersive bulk band in the vicinity of the Brillouin zone center $\overline{\Gamma}$. As we will see below, also a strongly dispersive surface state follows its band edge.

At an energy of −1.25 eV, an M-shaped region with a high spectral density shows up around $\overline{\Gamma}$. Along the $\overline{\mathrm{N}}$–$\overline{\Gamma}$–$\overline{\mathrm{N}}$ the dispersion is concave (bent upward, figure 2(a)) whereas along the $\overline{\mathrm{H}}$–$\overline{\Gamma}$–$\overline{\mathrm{H}}$ there is, in addition to the concave shape, a very small convex region (bent downward, figure 2(b)) very close to $\overline{\Gamma}$. This anisotropy has consequences for the dispersion of the Dirac-like surface state that is split off this bulk band.

Considering the spectral density of the topmost surface layer S, we find a surface state at −1.15 eV (experiment: about −1.2 eV), whose concave and weak dispersion follows that of the associated bulk band edge (this Dirac state is marked by an arrow in figure 2(c)). Along the $\overline{\mathrm{H}}$–$\overline{\Gamma}$–$\overline{\mathrm{H}}$, its dispersion becomes linear and much stronger than along the $\overline{\mathrm{N}}$–$\overline{\Gamma}$–$\overline{\mathrm{N}}$. It is this finding that is clearly reminiscent of the Dirac state in a topological insulator, say Bi_2Se_3. Due to the strong anisotropy of the dispersion, however, we can hardly speak of an isotropic Dirac *cone*.

When deliberately changing the inward relaxation δd_{12} of the top W layer S to zero, the Dirac point is shifted into the bulk band region at lower energies. This behavior is typical for a Shockley surface state that occurs due to a change of the crystal potential at the surface (rather than to a simple truncation of the infinite bulk system). From this finding we conclude that the surface relaxation is not essential for the appearance of the Dirac surface state. However, the inward relaxation 'pushes' the Dirac point into the bulk band gap. Hence, other heavy bcc(110) surfaces may show Dirac surfaces states as well.

As has been found in the experiment by Miyamoto *et al*, the Dirac state does not cross the band gap but displays a sharp maximum at $k = \pm 0.2\,a_0^{-1}$ and $E = -0.86$ eV (figure 2(d)). This change from an upward to a downward dispersion is explained by the strongly dispersive surface state that is associated with the bulk band edge mentioned above (marked 'surface state' in the figure). Both states belong to the same irreducible representation of the small group of $\boldsymbol{k}$ and, therefore, cannot cross. Their small distance in (E, k) results in a sizable hybridization which we will discuss by means of surface localization now.

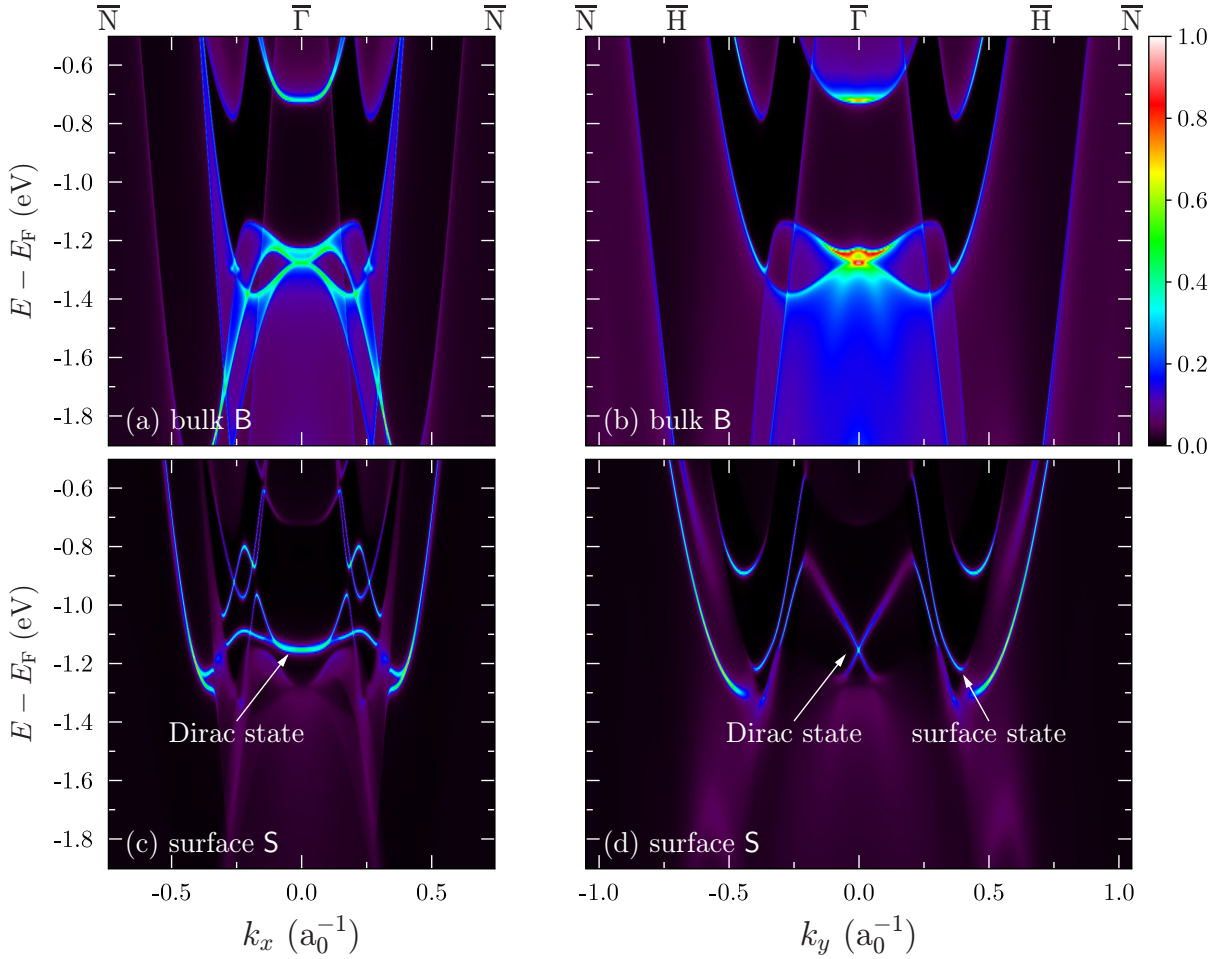

Figure 2. Spectral density of a bulk layer B (top row) and the topmost surface layer S (bottom row) along the $\overline{\text{N}}$–$\overline{\Gamma}$–$\overline{\text{N}}$ (left column) and the $\overline{\text{N}}$–$\overline{\text{H}}$–$\overline{\Gamma}$–$\overline{\text{H}}$–$\overline{\text{N}}$ (right column) lines of the two-dimensional Brillouin zone. The spectral densities are normalized and, thus, share a common color scale (right of panel (b)). The Dirac state and a surface state are marked by arrows. The wavenumber k is given in inverse Bohr radii, a_0^{-1}.

The spectral densities of the surface states become blurred when they appear in a region of bulk states, an indication of hybridization of surface and bulk states [39]. Another manifestation of hybridization but among surface states is their surface localization. Close to the Brillouin zone center $\overline{\Gamma}$, the Dirac state shows largest spectral weight in the topmost layer (filled triangles at layer S in figure 3) and decays monotonously toward the bulk without modulation. At larger wavenumbers, the Dirac state and the strongly dispersive surface state hybridize (figure 2(d)). As a consequence, they show similar properties: the spectral densities of these states, for example, are largest at layer S with almost identical size. However, their decay toward the bulk is slightly modulated, in contrast to the Dirac state at $\overline{\Gamma}$.

The linear dispersion of the Dirac state along $\overline{\text{H}}$–$\overline{\Gamma}$–$\overline{\text{H}}$ mimics that of a massless fermion. Along the $\overline{\text{N}}$–$\overline{\Gamma}$–$\overline{\text{N}}$ this state becomes ‘massive’, that is, it exhibits parabolic dispersion.

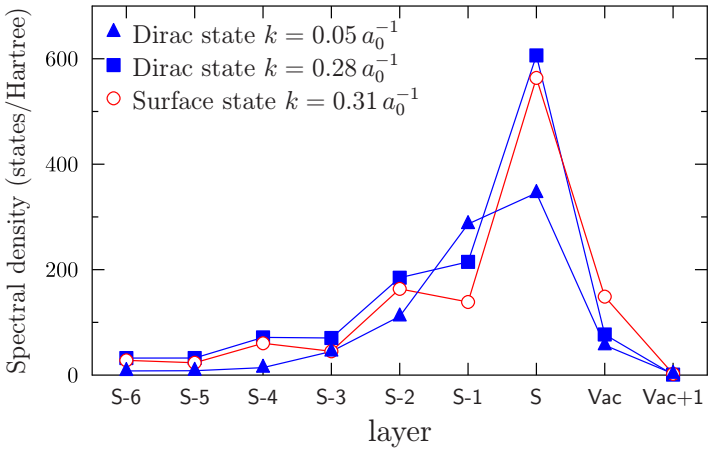

Figure 3. Surface localization of the Dirac state (blue filled symbols) and a surface state (red open circles). The energy is $E = -1.07$ eV; the wavevector is along the $\overline{\mathrm{H}} - \overline{\Gamma} - \overline{\mathrm{H}}$, with the wavenumber k indicated for each state in inverse Bohr radii (see figure 2(d)). S is the topmost surface layer; Vac indicates vacuum layers.

Hence, this strong anisotropy could be used to gradually increase or decrease the effective electron mass by changing the azimuth of the wavevector $\boldsymbol{k}$.

To elucidate the anisotropy of the dispersion in more detail, we present constant energy contours (CECs) of the spectral density in the surface layer S at selected energies (figure 4). At -1.0 eV, the Dirac state shows up as the inner rhombus that is elongated along k_x (the $\overline{\mathrm{N}}$–$\overline{\Gamma}$–$\overline{\mathrm{N}}$; figure 4(a)). This finding illustrates the weak dispersion in k_x and the strong dispersion in k_y. Due to the maximum in its dispersion (figure 2(d)), the Dirac state manifests itself in the CEC also as the innermost oval (indicated by an arrow as well). The strongly dispersive surface state shows up as the second innermost oval whose curvature follows closely that of the Dirac state. As a consequence, these states hybridize sizably in all $\boldsymbol{k}$ directions.

The anisotropy of the Dirac state's dispersion shows the importance of the third-order terms in the model Hamiltonian. It becomes even enhanced at lower energies, as is evident from the extremely elongated rhombus at -1.1 eV (figure 4(d)). Below the Dirac point but still above the bulk band region, for example at -1.2 eV, it appears that the spectral density shows weight only along k_x; see the almost parallel lines in figure 4(c). At even smaller energies, the hybridization of the Dirac state and bulk states results in a blurred spectral density (figure 4(b)).

At higher energies, a band gap opens up in the Dirac state along the $\overline{\mathrm{N}}$–$\overline{\Gamma}$–$\overline{\mathrm{N}}$ (cf -0.9 eV in figure 2(c)). This opening has the consequence that the Dirac state's rhombus and oval transform into two chevron-shaped features (figure 4(e)) that lie mirror symmetric with respect to the k_x-axis.

A comparison with experimental ARPES data, figure 3 in [11], establishes agreement with our calculations concerning the shape of the Dirac state's rhombohedral structure in the CECs. However, the ARPES measurements do not 'illuminate' the complete shape of the rhombus which is attributed to dipole selection rules in the photoemission process. Similar findings are reported by Winkelmann *et al* [36]. We will address this observation in section 3.3.

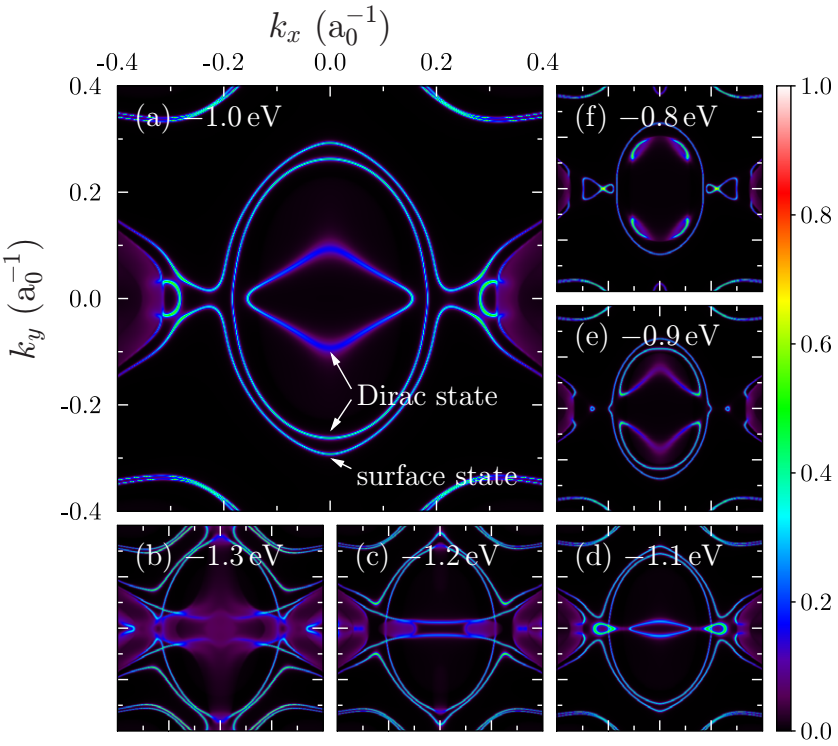

Figure 4. Spectral density in the topmost surface layer S around the center of the two-dimensional Brillouin zone for selected energies (relative to the Fermi energy, indicated in each panel). k_x is along the $\overline{\Gamma}$–$\overline{\mathrm{N}}$ and k_y is along the $\overline{\Gamma}$–$\overline{\mathrm{H}}$. The Dirac state and a surface state are marked by arrows in (a). The spectral densities are normalized and share a common color scale. All panels display the same region of the two-dimensional Brillouin zone, although (a) is enlarged.

3.2. Spin texture

The Rashba spin–orbit coupling implies a specific spin texture of the surface states. For an isotropic two-dimensional electron gas, the Rashba Hamiltonian yields a spin alignment within the confinement plane (here: xy or surface plane) and normal to the wavevector $\boldsymbol{k}$. For systems with threefold rotational symmetry, a tilt of the electron spin out-of-plane has been found: small for Au(111) [17] but as large as 45° for Bi_2Te_3 [40]. For W(110), however, the two orthogonal mirror planes in conjunction with time reversal forbid such an out-of-plane tilt (see section 2.1). Consequently, we focus on spin differences $s_\mu^\uparrow - s_\mu^\downarrow$ for an in-plane spin quantization axis normal to $\boldsymbol{k}$ (figure 5).

The Dirac state exhibits the expected spin texture that fully agrees with that derived from the model Hamiltonian. Interestingly, the strongly dispersive surface state that hybridizes with the Dirac state has a spin orientation opposite to that of the Dirac state (figure 5(b)). The degrees of spin polarization of the Dirac state are as large as 87.5% at $k = 0.05\,a_0^{-1}$ and 95.9% at $k = 0.28\,a_0^{-1}$ at $E = -1.07$ eV (i.e. at the (E, k) points used in 3); the surface state's spin polarization equals 86.8% at $k = 0.31\,a_0^{-1}$.

A similar observation has been made for the surface states in Bi/Cu(111) [15] and Bi/Ag(111) [16]. In these surface alloys, the Bi atoms induce two sets of surface states, one

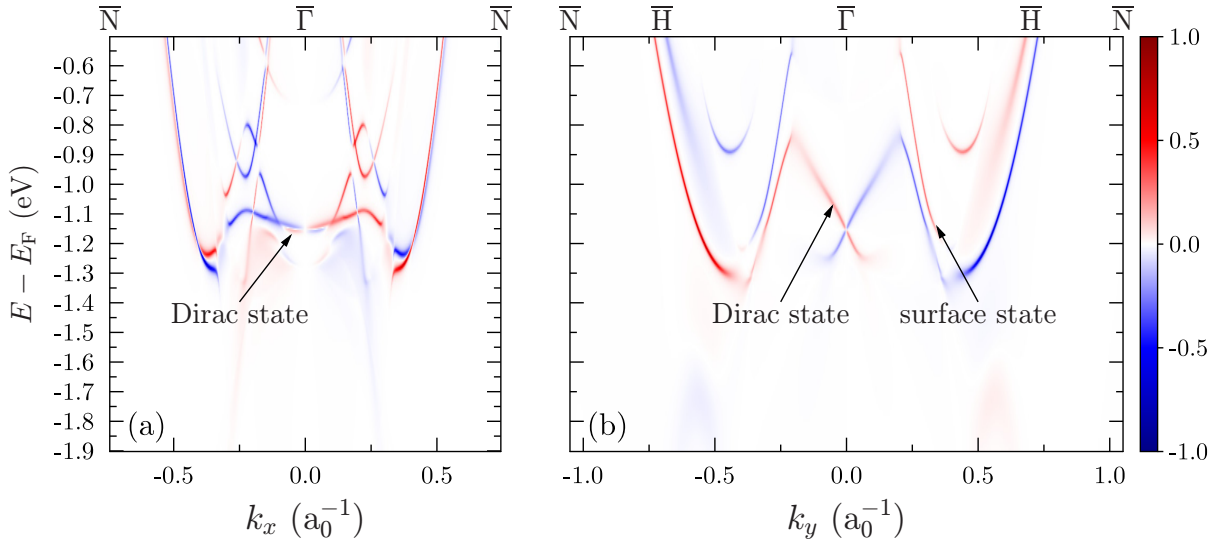

Figure 5. Spin-resolved electronic structure of the topmost surface layer S of W(110) along the $\overline{\text{N}}$–$\overline{\Gamma}$–$\overline{\text{N}}$ (a) and the $\overline{\text{N}}$–$\overline{\text{H}}$–$\overline{\Gamma}$–$\overline{\text{H}}$–$\overline{\text{N}}$ (b) lines of the two-dimensional Brillouin zone. The normalized spin differences $s_\mu^\uparrow - s_\mu^\downarrow$ are given as color scale (right of panel (b)); the spin quantization axis μ is in-plane and normal to the wavevector. The Dirac state and a surface state are marked by arrows.

at lower energy of mostly sp_z orbital composition and another one at higher energy with p_xp_y orbital composition. The outer branch of the lower set hybridizes with the inner branch of the upper set, both showing opposite spin polarization. For W(110), the strongly dispersive surface states play the role of the upper branch. The other electronic states at the surface are as well spin polarized due to spin–orbit coupling [41, 42].

Our findings reported so far corroborate the experimental observations and the conclusions drawn by Miyamoto *et al* [9, 11]. In particular, they support the surface origin of the spin-resolved properties. In turn, they contrast with a recent finding by Rybkin *et al* [43]: in their study on W(110), the spin-polarized features were attributed to bulk origin.

3.3. Spin- and angle-resolved photoelectron spectroscopy

Having analyzed the Dirac state in the previous sections, we now address how its properties manifest themselves in the photoemission intensities. Without spin–orbit coupling, electronic states are either even or odd with respect to mirror operations. With spin–orbit coupling, however, these components become mixed in the respective double group [19]. Furthermore, even spin-up orbitals can hybridize with odd spin-down orbitals and vice versa, as has been found in Bi/Cu(111) [15]. As a result, the spin polarization is less than 100%. Since the spatial character of the initial state in the photoemission process can be selected by the polarization of the incident light, one could observe a reversal of the spin texture upon changing from s-polarized light to p-polarized light.

We will now address this effect for the $\overline{\text{H}}$–$\overline{\Gamma}$–$\overline{\text{H}}$ azimuth. For s-polarized light, the vector potential $\boldsymbol{A}$ of the incident light lies parallel to the surface plane and normal to the yz plane.

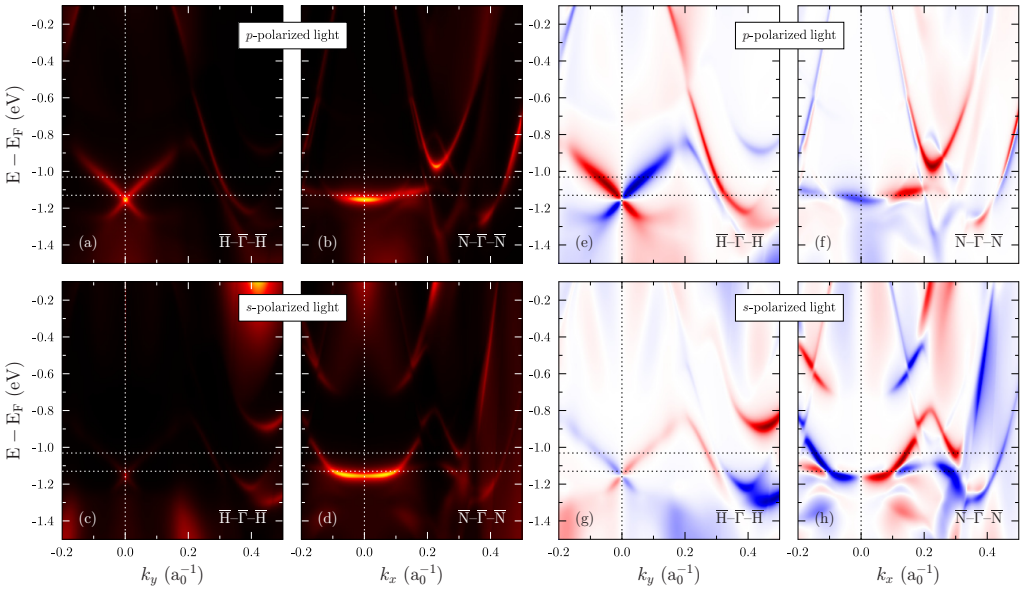

Figure 6. Spin-integrated (a)–(d) and spin-resolved (e)–(h) photoemission intensities from W(110) along the $\overline{\mathrm{H}}$–$\overline{\Gamma}$–$\overline{\mathrm{H}}$ and $\overline{\mathrm{N}}$–$\overline{\Gamma}$–$\overline{\mathrm{N}}$. The polarization of the incident light is shown for each panel. Blue and red indicate opposite (in-plane) spin directions. The maximum degrees (darkest blue) are 86% (e), 33% (f), 92% (g) and 76% (h); the minimum degrees of spin polarization (darkest red) are −88% (e), −98% (f), −94% (g) and −76% (h).

Hence, only A_x is nonzero and $\boldsymbol{A}$ is odd under m_{yz} (table 1). Therefore, only odd orbitals under m_{yz} can be probed. For p-polarized light, $\boldsymbol{A}$ is even under m_{yz} and even orbitals are probed.

The spectral-density calculations yield that the Dirac state near $\overline{\Gamma}$ is mainly of d_{z^2} orbital character which is even under m_{yz}. Consequently, its photoemission intensity is large for p-polarization (figure 6(a)) and small for s-polarization (c). As suggested before, we find the expected spin reversal: the Dirac state at $k_y > 0$ is spin-up (blue in figure 6(e)) for p-polarization but spin-down (red in figure 6(g)) for s-polarization. As found already in figure 5(g), the highly dispersive surface state shows a spin polarization opposite to that of the Dirac state.

Analogous considerations hold for the $\overline{\mathrm{N}}$–$\overline{\Gamma}$–$\overline{\mathrm{N}}$ azimuth (figures 6(b) and (d)). Similar to the $\overline{\mathrm{H}}$–$\overline{\Gamma}$–$\overline{\mathrm{H}}$ azimuth, the strongly dispersive surface state is observed for p-polarized light but is absent for s-polarized light, which implies that this state is even with respect to the mirror operation m_{xz}. The flattened states shown along k_x consist of even and odd states. For p-polarized light, the flattened states show a larger intensities near the center of the Brillouin zone and fade out for larger k. The situation is reversed for s-polarized light: intensities are weaker close to the center of the Brillouin zone and become stronger for larger momenta.

The experiments by Miyamoto *et al* [11] reveal a rather strong sensitivity of the Dirac state's intensity on the electron detection direction: for negative k (along $\overline{\mathrm{H}}$–$\overline{\Gamma}$–$\overline{\mathrm{H}}$), the Dirac state shows up clearly but is suppressed for positive k (cf state S_1 in figure 2(a) of their publication). Our computations do not show such a strong asymmetry, a finding that is easily understood from the Dirac state's orbital character (mostly d_{z^2}). To resolve this issue, we would like to suggest detailed experimental and theoretical investigations that include a spin analysis of the photocurrent.

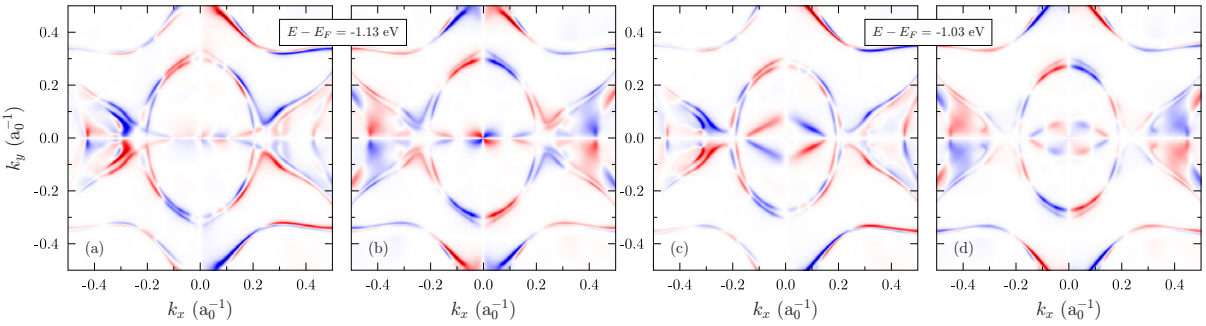

Figure 7. Spin-resolved photoemission intensities from W(110) at constant initial energies, as indicated. Panels (a) and (c) ((b) and (d)) show results for p-polarized (s-polarized) light. The red–white–blue color scale represents negative–zero–positive out-of-plane spin differences s_z for polar scans in the azimuth range from -90° to $+90^\circ$. The maximum degrees of spin polarization (darkest blue) are 55% (a), 62% (b), 66% (c) and 65% (d). The minimum degrees of spin polarization (darkest red) are the same values but with opposite sign, due to the symmetry of the setup.

The spin polarization of the Dirac state lies within the surface plane of all $\boldsymbol{k}$, as is shown in the previous section. The complete in-plane spin polarization of the (initial) Dirac surface state is due to the joint effect of rotation and time-reversal invariance. The photoemission process, however, breaks the time-reversal symmetry; as a consequence, the restriction induced by time reversal on the spin polarization (operation T in table 1) is no longer valid, and the out-of-plane component of the photoelectron's spin polarization can be nonzero for $\boldsymbol{k}$ that do not lie within a mirror plane.

To investigate the out-of-plane spin component that is induced by the photoemission process itself, we have computed spin-resolved ARPES maps at constant energies (figure 7). The intensities have been obtained for polar-angle scans, with the azimuth running from -90° to $+90^\circ$; this is the setup as sketched in figure 1 of [9].

For both light polarizations, s_z vanishes in a mirror plane of the surface (see table 1). However, the spin-resolved intensity patterns of s- and p-polarized light differ in their symmetry. For s-polarized light, s_z shows twofold rotational symmetry (figures 7(b) and (d)); by crossing a mirror plane, it changes sign (the same holds for the in-plane spin polarization (not shown)). However, for off-normally incident p-polarized light (figures 7(a) and (c)), the twofold symmetry is broken but s_z changes sign when turning k_y into $-k_y$ for fixed k_x. This result is fully in line with table 1 (cf the effect of the operation m_{xz} on s_z). Also the in-plane components s_x and s_y comply with table 1. The out-of-plane spin polarization is as large as 92% at $k = (0.004, 0.008)\ a_0^{-1}$ in figure 7(b) and 44% at $k = (0.098, 0.044)\ a_0^{-1}$ in figure 7(c). Note that these numbers depend on the chosen lifetime broadening; a larger lifetime broadening would reduce these values. We conclude that if a spin polarization component is not forbidden by symmetry it is actually nonzero. Evidently, its degree and sign depend on the transition matrix elements that are calculated from realistic initial and final states and consequently depend on the specific setup.

We would like to emphasize that the purpose of the present SARPES calculations is to show the major effects concerning the spin polarization of photoelectrons excited from the Dirac surface state. For this reason we used the setup detailed in the publications by

Miyamoto *et al* [9, 11]. Nevertheless, we performed additional photoemission calculations using different setups: with fixed incidence angles of 20° and 50° with respect to the sample. To check the effect of the final states, we performed calculations for different photon energies as well. As a result in both cases, the photoemission intensities from the Dirac surface state and its out-of-plane spin polarization change.

4. Concluding remarks

The d_{z^2} surface state in W(110) shows a rich variety of features which are brought about by the spin–orbit interaction. Although most of its properties that have been determined experimentally by photoelectron spectroscopy [9, 11] are explained in the present theoretical investigation, there remain a very few issues to be solved in future studies. For example, the strong asymmetry of the experimental photoemission intensities is not fully supported by our calculations. On the other hand, the out-of-plane spin polarization that is brought about by the photoemission process itself calls for an experimental investigation by spin-resolved photoelectron spectroscopy.

The observation of a Dirac-like surface state at a metal surface opens another 'playground' for spin–orbit-induced phenomena, besides the well-understood surface alloys on Ag(111) and Cu(111) (e.g. Bi/Ag(111) [14]) and the emerging field of strong topological insulators.

Acknowledgments

We are very grateful to M Donath (U Münster) and R Feder (U Duisburg-Essen) for stimulating and fruitful discussions.

References

[1] Hasan H and Kane C 2010 Colloquium: topological insulators *Rev. Mod. Phys.* **82** 3045
[2] Hsieh D *et al* 2009 Observation of time-reversal-protected single-Dirac-cone topological-insulator states in Bi_2Te_3 and Sb_2Te_3 *Phys. Rev. Lett.* **103** 146401
[3] Fu L 2009 Hexagonal warping effects in the surface state of the topological insulator Bi_2Te_3 *Phys. Rev. Lett.* **103** 266801
[4] König M, Wiedmann S, Brüne C, Roth A, Buhmann H, Molenkamp L W, Qi X-L and Zhang S-C 2007 Quantum spin Hall insulator state in HgTe quantum wells *Science* **318** 766
[5] Zhang H, Liu Ch-X, Qi X-L, Fang Zh and Zhang Sh-Ch 2009 Topological insulators in Bi_2Se_3, Bi_2Te_3 and Sb_2Se_3 with a single Dirac cone on the surface *Nature Phys.* **5** 438
[6] Eremeev S V *et al* Atom-specific spin mapping and buried topological states in a homological series of topological insulators *Nature Commun.* **3** 635
[7] Di Sante D, Barone P, Bertacco R and Picozzi S 2013 Electric control of giant Rashba effect in bulk GeTe *Adv. Mater.* **25** 509
[8] Chadov St, Kiss J, Felser C, Chadova K, Ködderitzsch D, Minár J and Ebert H 2012 Topological phase transition induced by random substitution arXiv:1207.3463v1
[9] Miyamoto K, Kimura A, Kuroda K, Okuda T, Shimada K, Namatame H, Taniguchi M and Donath M 2012 Spin-polarized Dirac-cone-like surface state with *d* character at W(110) *Phys. Rev. Lett.* **108** 066808
[10] Jung W *et al* 2011 Warping effects in the band and angular-momentum structures of the topological insulator Bi_2Te_3 *Phys. Rev.* B **84** 245435

[11] Miyamoto K, Kimura A, Kuroda K, Okuda T, Shimada K, Iwasawa H, Hayashi H, Namatame H, Taniguchi M and Donath M 2012 Massless or heavy due to two-fold symmetry: surface-state electrons at W(110) *Phys. Rev.* B **86** 161411
[12] Bychkov Y A and Rashba E I 1984 Oscillatory effects and the magnetic susceptibility of carriers in inversion layers *J. Phys. C: Solid State Phys.* **17** 6039
[13] Winkler R 2003 *Spin–Orbit Coupling Effects in Two-Dimensional Electron and Hole Systems* (Berlin: Springer)
[14] Ast Chr R, Henk J, Ernst A, Moreschini L, Falub M C, Pacilé D, Bruno P, Kern K and Grioni M 2007 Giant spin splitting through surface alloying *Phys. Rev. Lett.* **98** 186807
[15] Mirhosseini H, Henk J, Ernst A, Ostanin S, Chiang C-T, Yu P, Winkelmann A and Kirschner J 2009 Unusual spin topology of unoccupied spin–orbit split surface states in surface alloys *Phys. Rev.* B **79** 245428
[16] Bentmann H, Abdelouahed S, Mulazzi M, Henk J and Reinert F 2012 Direct observation of interband spin–orbit coupling in a two-dimensional electron system *Phys. Rev. Lett.* **108** 196801
[17] Henk J, Hoesch M, Osterwalder J, Ernst A and Bruno P 2004 Spin–orbit coupling in the L-gap surface states of Au(111): spin-resolved photoemission experiments and first-principles calculations *J. Phys.: Condens. Matter* **16** 7581
[18] Vajna Sz, Simon E, Szilva A, Palotas K, Ujfalussy B and Szunyogh L 2012 Higher-order contributions to the Rashba–Bychkov effect with application to the Bi/Ag(111) surface alloy *Phys. Rev.* B **85** 075404
[19] Inui T, Tanabe Y and Onodera Y 1990 *Group Theory and its Applications in Physics* (*Springer Series in Solid State Sciences* vol 78) (Berlin: Springer)
[20] Premper J, Trautmann M, Henk J and Bruno P 2007 Spin–orbit splitting in an anisotropic two-dimensional electron gas *Phys. Rev.* B **76** 073310
[21] Simon E, Szilva A, Ujfalussy B, Lazarovits B, Zarand G and Szunyogh L 2010 Anisotropic Rashba splitting of surface states from the admixture of bulk states: relativistic *ab initio* calculations and $k \cdot p$ perturbation theory *Phys. Rev.* B **81** 235438
[22] Henk J 2002 Theory of low-energy diffraction and photoelectron spectroscopy from ultra-thin films *Handbook of Thin Film Materials* vol 2 ed H S Nalwa (San Diego, CA: Academic) chapter 10, p 479
[23] Zabloudil J, Hammerling R, Szunyogh L and Weinberger P (ed) 2005 *Electron Scattering in Solid Matter* (Berlin: Springer)
[24] Perdew J P and Wang Y 1992 Accurate and simple analytic representation of the electron-gas correlation energy *Phys. Rev.* B **45** 13244
[25] Weinberger P 1990 *Electron Scattering Theory of Ordered and Disordered Matter* (Oxford: Clarendon)
[26] Rundgren J and Malmström G 1977 Transmission and reflection of low-energy electrons at the surface barrier of a metal *J. Phys. C: Solid State Phys.* **10** 4671–87
[27] Giebels F, Gollisch H and Feder R 2013 Electron pair emission from W(110): Response to a spin-polarized surface state *Phys. Rev.* B **87** 035124
[28] Meyerheim H L, Sander D, Popescu R, Steadman P, Ferrer S and Kirschner J 2001 Interlayer laxation of W(110) studied surface x-ray diffraction *Surf. Sci.* **475** 103
[29] Venus D, Cool S and Plihal M 2000 Quantitative structural determination using spin-polarized low-energy electron diffraction rotation curves: W(110) *Surf. Sci.* **446** 199
[30] Braun J 1996 The theory of angle-resolved ultra-violet photoemission and its applications to ordered materials *Rep. Prog. Phys.* **59** 1267
[31] Feibelman P J and Eastman D E 1974 Photoemission spectroscopy—correspondence between quantum theory and experimental phenomenology *Phys. Rev.* B **10** 4932
[32] Schattke W 1997 Photoemission within and beyond the one-step model *Prog. Surf. Sci.* **54** 211
[33] Rose E M 1961 *Relativistic Electron Theory* (New York: Wiley)
[34] Heinzmann U and Dil J H 2012 Spin–orbit-induced photoelectron spin polarization in angle-resolved photoemission from both atomic and condensed matter *J. Phys.: Condens. Matter* **24** 173001

[35] Hermanson J 1977 Final-state symmetry and polarization effects in angle-resolved photoemission spectroscopy *Solid State Commun.* **22** 9–11
[36] Winkelmann A, Tusche Chr, Akin Ünal A, Ellguth M, Henk J and Kirschner J 2012 Analysis of the electronic structure of copper via two-dimensional photoelectron momentum distribution patterns *New J. Phys.* **14** 043009
[37] Braun J and Donath M 2004 Theory of photoemission from surfaces *J. Phys.: Condens. Matter* **16** S2539
[38] Seah M P and Dench W A 1979 Quantitative electron spectroscopy of surfaces: a standard data base for electron inelastic mean free paths in solids *Surf. Interface Anal.* **1** 2
[39] Akin Ünal A, Tusche Chr, Quazi S, Wedekind S, Chiang C-T, Winkelmann A, Sander D, Henk J and Kirschner J 2011 Hybridization between the unoccupied Shockley surface state and bulk electronic states on Cu(111) *Phys. Rev.* B **84** 073107
[40] Henk J, Ernst A, Eremeev S V, Chulkov E C, Maznichenko I V and Mertig I 2012 Complex spin texture in the pure and Mn-doped topological insulator Bi_2Te_3 *Phys. Rev. Lett.* **109** 036803
[41] Kimura A *et al* 2010 Strong Rashba-type spin polarization of the photocurrent from bulk continuum states: experiment and theory for Bi(111) *Phys. Rev. Lett.* **105** 076804
[42] Krasovskii E E and Chulkov E V 2011 Rashba polarization of bulk continuum states *Phys. Rev.* B **83** 155401
[43] Rybkin A G, Krasovskii E E, Marchenko D, Chulkov E V, Varykhalov A, Rader O and Shikin A M 2012 Topology of spin polarization of the 5*d* states on W(110) and Al/W(110) surfaces *Phys. Rev.* B **86** 035117